Implementation of an advanced bounding surface constitutive model in OpenSees

Tony Fierro [a,*], Stefano Ercolessi [a], Davide Noè Gorini [b], Giovanni Fabbrocino [a,c], Filippo Santucci de Magistris [a]

[a] *University of Molise, via De Sanctis 1, Campobasso 86100, Italy*
[b] *Sapienza University of Rome, Rome, Italy*
[c] *ITC-CNR, L'Aquila Branch, Via G. Carducci, 67100 L'Aquila, Italy*

ARTICLE INFO

ABSTRACT

The dynamic behaviour of saturated coarse-grained soils has recently received wide attention because of its impact on the seismic performance of geotechnical and structural systems. This is due to the peculiarities of their cyclic response (e.g., liquefaction, ratcheting and volumetric-deviatoric coupling). Consequently, the seismic risk mitigation of the built environment requires efficient predictive models applicable in design and assessment. To this end, several constitutive models have been developed for a realistic description of the cyclic soil behaviour. From this perspective, this paper describes the implementation and testing of the bounding surface plasticity model developed by Papadimitriou and Bouckovalas (2002) in OpenSees as a means for advanced assessment of soil-structure systems. The implemented model includes essential features of the cyclic soil response. Moreover, a modified fabric tensor evolution equation is introduced for improving the response and numerical stability in boundary value problems, at the cost of an extra model constant. The workflow concerning the integration of the model into OpenSees is presented, followed by instructions about its use in boundary value problems. A comprehensive verification of the model response is discussed. The numerical simulations demonstrated the robustness of the implemented code in capturing soil behaviour from small to large strain levels.

1. Introduction

As a key element for a reliable assessment of geotechnical systems undergoing large deformations, an accurate description of the dynamic response of coarse-grained soils still represents a challenging issue in earthquake engineering. The cyclic soil behaviour is indeed characterised by salient features, such as the cycle-by-cycle degradation in shear stiffness and the regain of shear stiffness and strength manifested under increasingly larger shear strain excursions. As a consequence, several constitutive models have been developed over the years according to different analytical frameworks. A fruitful compromise between the accuracy of the numerical predictions and direct applicability to boundary value problems is represented by meso-scale constitutive models, which have mainly been developed within the framework of multi-surface plasticity (Prevost, 1978; Yang et al., 2003; Yang and Elgamal, 2008), generalised plasticity (Pastor et al., 1990; Ling and Liu, 2003), hypo-plasticity (Niemunis and Herle, 1997; Mašín, 2014) or bounding surface plasticity (Manzari and Dafalias, 1997; Papadimitriou

and Bouckovalas, 2002; Limnaiou and Papadimitriou, 2022).

Bounding surface plasticity turned out to be particularly effective in describing soil response, under both monotonic and cyclic loading, from the scale of the elemental volume to large domains. The combination of the Critical State theory (Schofield and Wroth, 1968) with the concept of bounding surface plasticity (Dafalias and Popov, 1975; Dafalias, 1986) represents a recurrent feature of the analytical formulation. Wood et al. (1994) provided a unified indicator of these concepts by expressing the peak stress ratio, i.e., the ratio q/p' of the maximum deviatoric stress to the mean effective stress, as a function of the state parameter $\Psi = e - e_{cs}$ (Been and Jeffries, 1985), where e is the current void ratio and e_{cs} is the corresponding Critical State value at the current p'. In addition, to reproduce likely dilatancy-related effects on the stiffness and strength properties of coarse-grained soils, Manzari and Dafalias (1997) proposed a two-surface, bounding surface model employing the concept of Phase Transformation Line (PTL) developed by Ishihara et al. (1975). The analytical framework was validated with reference to a sandy soil under both drained and undrained conditions. The bounding surface

framework was further developed in numerous subsequent studies. Among others, Papadimitriou and Bouckovalas (2002) and Dafalias and Manzari (2004) introduced the effect of fabric evolution in the hardening regime through the definition of a specific tensorial fashion, validating the improved formulation against experimental data of Nevada and Toyoura sands. Furthermore, in Papadimitriou and Bouckovalas (2002), the formulation was augmented with i) an empirical index directly scaling the plastic modulus to consider fabric effects on the hardening response of the soil and ii) a Ramberg–Osgood nonlinear elastic formulation in the small-strain regime.

By virtue of a manageable analytical framework, the above bounding surface plasticity models were implemented in numerical codes and efficiently used in advanced simulations of the responses of large-scale soil-structure systems. In fact, the Dafalias and Manzari (2004) model, commonly known as SANISAND, was implemented in a number of frameworks, such as Plaxis (Brinkgreve et al., 2021) by Martinelli et al. (2015), and OpenSees (McKenna et al., 2010) by Ghofrani and Arduino (2016), to simulate boundary value problems. This initiated research- and practice-oriented developments in the field, such as constitutive models based on the PM4Sand framework, describing the plane-strain cyclic response of sandy and silty soils (Boulanger and Ziotopoulou, 2017; Boulanger and Ziotopoulou, 2019).

To the authors' knowledge, the model by Papadimitriou and Bouckovalas (2002) was implemented in FLAC (Itasca, 2019) by Andrianopoulos et al., (2010a), a version known as NTUA-SAND, that introduced the following modifications into the formulation. A vanishing yield surface was considered in lieu of the narrow yield surface surrounding the current stress state in the original version, and an adaptable stress projection related to the last load reversal was introduced as a mapping rule. In particular, the latter is a typical feature of the so-called SANISAND-R constitutive models (see Papadimitriou et al., 2019, for a complete description), where the suffix "R" stands for "reversal surfaces". In this view, the original formulation of the model by Papadimitriou and Bouckovalas (2002) is regarded as a SANISAND-type model because the last load reversal is not introduced in the mapping rule. Further modifications implemented in NTUA-SAND with respect to the original model consist of the interpolation rule and the fabric tensor evolution laws. NTUA-SAND efficiently simulates a wide range of boundary value problems, namely, the response of a footing resting on a liquefiable deposit (Karamitros et al., 2013a, 2013b; Dimitriadi et al., 2017; 2018), the lateral spreading of piled foundations (Chaloulos et al., 2013; 2014), the effectiveness of soil improvement techniques (Papadimitriou et al., 2021; Papadimitriou et al., 2022), and the uplift of buried pipelines induced by soil liquefaction (Marinatou et al., 2017). Although the results shown in those studies are very promising with regard to predicting the evolution of the effective stress–strain response and liquefaction triggering, the original formulation is not available in any numerical environment. In fact, it was implemented in Abaqus by Miriano (2010) and Miriano et al. (2016) as an external subroutine, not included in the official release, to simulate the response of an anchored diaphragm under drained conditions. However, the source code was not published, limiting its practical impact.

In light of the above, this paper presents a detailed workflow for the implementation and use of the Papadimitriou and Bouckovalas (2002) model in the open-source, finite-element analysis framework OpenSees (McKenna et al., 2010) as an essential step for its application in earthquake-related problems.

The paper is structured as follows: Section 2 describes the main aspects of the analytical framework of the reference model. Section 3 explains the model implementation in OpenSees, providing details regarding the adopted procedure, the integration schemes and additional guidelines for its use in finite element simulations. In Section 4, the implementation is verified at the element level by comparing the model response with those related to the existing implementations. Section 5 describes i) the edit introduced into the formulation to improve both the model response and the numerical stability in

boundary value problems, ii) the performance of the new source code with respect to the dynamic response of a liquefiable soil deposit, comparing it with experimental data and the SANISAND response. Finally, Section 6 provides concluding remarks.

2. The Papadimitriou and Bouckovalas (2002) constitutive model

The Papadimitriou and Bouckovalas (2002) model represents the multiaxial generalisation of the bounding surface constitutive framework developed by Papadimitriou et al. (2001), with slight changes detailed later in the section. Here, the model is referred to as NTUA-Sand02 to distinguish it from the modified version of the model, NTUA-SAND (Andrianopoulos et al., 2010a). Although the main characteristics of NTUASand02 are recalled in the following, the reader can refer to Papadimitriou and Bouckovalas (2002) for a more comprehensive description.

The state of soil is determined by means of the state parameter $\Psi = e - e_{cs}$ by Been and Jeffries (1985), where the void ratio at Critical State varies with the effective stress through the following logarithmic function:

$$e_{cs} = (e_{cs})_a - \lambda \ln\left(\frac{p'}{p_{atm}}\right) \tag{1}$$

where p' and p_{atm} are the effective mean and atmospheric pressure, respectively, and $(e_{cs})_a$ and λ are model constants to be calibrated using standard monotonic laboratory tests (Papadimitriou et al., 2001).

The plastic response develops when the current stress state lies on the conical yield surface surrounding it and the stress increment is directed outwards from the surface. The evolution of the hardening response is controlled by the distance between the current stress state and the three surfaces of dilatancy, Critical State, and bounding, according to the mapping rule schematically shown in Fig. 1a. Each surface is described by a cone with the apex at the origin of the stress space (Fig. 1a). The projection of these surfaces on the π-plane is shown in Fig. 1b, where r_i indicates the deviatoric stress ratio between the ith principal effective stress, s_i, and the mean effective stress, p'. The conical yield surface is defined through the back-stress ratio tensor α, which defines its inclination with respect to the hydrostatic axis, and by the parameter m defining its size. Except for the Critical State surface, the other surfaces evolve in the stress space according to a kinematic hardening law controlling the evolution of α (rotation of the yield surface) when plastic strains occur.

The other surfaces present the same wedge-shaped formulation in the π -plane and have different slopes in the p'-q plane (q = deviatoric stress) in compression and extension; that is, $M_c^i \neq M_e^i$, with i = c,b, d representing the Critical State, bounding and dilatancy surfaces, respectively. These stress ratios are interrelated as $M_{c,e}^b = M_{c,e}^c + k_{c,e}^b \langle -\psi \rangle$ and $M_{c,e}^d = M_{c,e}^c + k_{c,e}^d \psi$, where k_c^b and k_c^d are model constants and $k_e^{b,d} = \frac{M_e^c}{M_c^c} k_c^{b,d}$.

In addition to the stresses and strains, the internal (state) variables listed in Table 1 are the tensor α, the void ratio e and the fabric tensor $\mathbf{F}$. The non-associativity of the flow rule is restricted to its volumetric component. Along the lines of bounding surface plasticity models (Manzari and Dafalias, 1997), the distances between the back-stress ratio α and its image on the model surfaces projected along the $\mathbf{n}$ direction are defined as:

$$d^i = \left(\boldsymbol{\alpha}^i - \boldsymbol{\alpha}\right) : \mathbf{n} \tag{2}$$

in which $\boldsymbol{\alpha}^i$ is referred to as the image back-stress ratio tensor, i.e., the image points of the current back-stress ratio on the bounding (i = b), Critical State (i = c), and dilatancy (i = d) surfaces, while tensor $\mathbf{n}$ is the outward normal to the yield surface, collinear to $\mathbf{r}$- $\boldsymbol{\alpha}$. The size of the
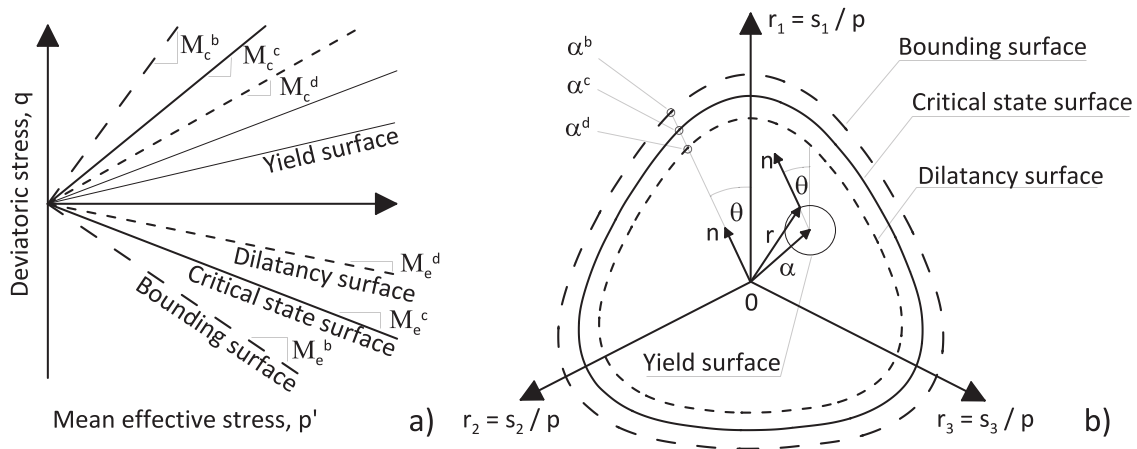
Fig. 1. Constitutive framework in both triaxial (a) and deviatoric (b) planes (from Papadimitriou and Bouckovalas, 2002).

Table 1
NTUASand02 constitutive parameters, with values calibrated for Nevada sand as proposed by Papadimitriou and Bouckovalas (2002), and state variables.

Parameter	Meaning	Value	Tcl syntax
$(e_{cs})_a$	CSL Location in the e-ln(p) space	0.809	$ecs_a
λ	CSL Location in the e-ln(p) space	0.022	$lambda_c
M_c^c	Critical state strength in triaxial compression	1.25	$Mc
M_e^c	Critical state strength in triaxial extension	0.9	$Me
B	Elastic shear modulus constant	200 – 520*	$B
a_1	Non-linearity of the elastic shear modulus	0.67	$a1
γ_1	Strain limit of elastic modulus degradation	0.00025	$gamma1
ν	Poisson's ratio	0.31	$nu
k_c^b	Effect of Ψ on peak stress ratio	1.45	$k_bc
k_c^d	Effect of Ψ on stress ratio at PT	0.3	$k_dc
A_o	Dilatancy constant	2.1	$A0
h_o	Plastic modulus constant	5000	$h0
H_o	Fabric index constant	68000	$H0
ς	Effect of major principal stress on fabric index	1.0	$zeta
m	Yield surface constant	0.0625	$m
$\boldsymbol{\sigma}$	Stress tensor (state variable)		
$\boldsymbol{\varepsilon}$	Strain tensor (state variable)		
$\boldsymbol{\alpha}$	Back-stress ratio tensor (state variable)		
$\mathbf{F}$	Fabric tensor (state variable)		
e	Current void ratio (state variable)		

* Values used under monotonic and cyclic conditions, respectively.

surfaces depends on the state parameter, whereas their shape is controlled by the Lode angle θ based on a radial mapping rule. The latter is formulated in terms of stress ratio tensor invariants $\bar{\mathbf{r}} = \mathbf{r} - \boldsymbol{\alpha}$. Consequently, these three surfaces are expressed as:

$$\boldsymbol{\alpha^i} = \sqrt{2/3}\alpha_\theta^i \mathbf{n} \tag{3}$$

where $\alpha_\theta^i = g(\theta, c^i)M_c^i - m$ and $g(\theta, c^i)$ is an interpolation function of the Lode angle and of the ratio $c^i = M_e^i/M_c^i$.

Two novel aspects of the model are represented by the nonlinear Ramberg–Osgood formulation to simulate more realistically the small-strain soil behaviour (elastic regime), differently from much more commonly used linear elastic relationships, and by the definition of a scalar parameter, h_f, scaling the plastic modulus to consider the fabric tensor evolution (Papadimitriou and Bouckovalas, 2002).

According to the nonlinear Ramberg–Osgood formulation, the elastic shear and bulk moduli, G_t and K_t, respectively, are functions of the mean effective stress, the void ratio, Poisson's ratio and a scalar variable T that

introduces shear modulus degradation as a function of the distance between the current deviatoric stress ratio (**r**) and its value at the last load reversal ($\mathbf{r}_{ref}$) on the π -plane (Papadimitriou and Bouckovalas, 2002).

The scalar parameter h_f acts as a macroscopic effect on the plastic strain rate of the fabric evolution occurring in the micro-structure of sandy soils during shearing. It is given as:

$$h_f = \frac{1 + \langle \mathbf{F} : \mathbf{I} \rangle^2}{1 + \langle \mathbf{F} : \mathbf{n} \rangle} = \frac{1 + \langle f_p \rangle^2}{1 + \langle \mathbf{f} : \mathbf{n} \rangle} \tag{4}$$

where **f** and f_p indicate the deviatoric and volumetric parts of the fabric tensor **F**, respectively. The plastic modulus, K_p, is defined as:

$$K_p = p \cdot h_b \cdot h_f \cdot d^b \tag{5}$$

The plastic modulus K_p depends closely on the distance d^b (see Eq. (2); also enclosed in the scalar variable h^b) and becomes negative when $d^b < 0$ to simulate deviatoric stress-ratio softening. This feature implies that the bounding surface can be crossed by the current stress state, as originally proposed by Manzari and Dafalias (1997).

The NTUASand02 formulation requires the definition of the 15 parameters reported in Table 1. The relative values in the table refer to the calibration carried out by Papadimitriou and Bouckovalas (2002) for Nevada sand against the experimental data of the VELACS project (Arulmoli et al., 1992).

3. Implementation in OpenSees

3.1. General structure of the source code and incremental response

The features discussed in the previous section make NTUASand02 particularly suitable for simulating the cyclic response of coarse-grained soils from small- to large-strain levels. Therefore, the model was implemented as a new multiaxial material in the open-source analysis framework OpenSees (McKenna et al., 2010); this platform is continuously under development for advanced assessment of soil-structure systems subjected to natural hazards. The source code is composed of two C++ files: a header file, where all the functions and variables are declared to make the new feature communicating with the others in the framework, and a main file developing the functions that compute the material current state and the incremental response. The set of functions that form the code are described in Appendix A, while only the ones directly invoked in the computation of the incremental response are reported below.

In solving the incremental response, in the main file of NTUASand02, the stress, strain, fabric, and back-stress ratio tensors are initialised; that is, the fabric and back-stress ratio tensors are set as null tensors, whereas the stress tensor is set as hydrostatic with diagonal elements assuming

the cut-off value of the mean effective pressure p_{min}', the latter taken as 10^{-4} times the atmospheric pressure. This represents a lower bound required for numerical stability to avoid the unacceptable condition $p' \leq 0$, typically occurring for sandy soils under undrained cyclic loading. The selected value for p_{min}' was compatible with that chosen by Taborda et al. (2014).

Once the analysis begins, the trial strain is taken from the deformations of the finite element through the function *setTrialStrain*, which is fully developed in external C++ files available in the OpenSees framework. Once the trial strain tensor is obtained, the function *integrate* is recalled, where the integration type is selected based on a switch that takes the value assigned to the command *updateMaterialStage* in the script of the finite element analysis. The integration can be performed using either the elastic (*updateMaterialStage* = 0 implies that the function *elastic_integrator* is used) or the elastic–plastic tangent stiffness matrix (*updateMaterialStage* = 1, corresponding to the function *explicitIntegrator*). In the latter case, the full elastic–plastic formulation is activated. Different explicit integration schemes can be adopted for the elastic–plastic integration, as discussed in the next section. At the end of each analysis step, the stress, strain, back-stress ratio and fabric tensors are computed according to the constitutive relationships. The procedure iterates until convergence is attained, where the state variables are committed and represent the initial values for the successive analysis step.

3.2. Integration schemes

The hardening rule and the plastic potential gradient are integrated into the code by adopting explicit schemes. For the NTUASand02 material, three explicit algorithms are implemented: Forward Euler, Modified Euler with substepping (Sloan et al., 2001), and 4th-order Runge-Kutta. The Modified Euler scheme is set as the default as a good compromise between accuracy and computational time. A concise description of the key features of the algorithms is provided. In addition, the reader can refer to Sloan et al. (2001), Anandarajah (2011), Ghofrani (2018), Chen and Arduino (2021) and Fierro (2022) for further details.

In the Modified Euler scheme, the strain increment $\dot{\varepsilon}$ obtained from the finite element can be divided into a number of subincrements $\dot{\varepsilon}_n$ so that the integration refers to the pseudo-time interval $\Delta T_n = T_n - T_{n-1}$ (where $0 \leq \Delta T_n \leq 1$) as:

$$\dot{\varepsilon}_n = \Delta T_n (\dot{\varepsilon}) \tag{6}$$

Hence, the explicit Euler method performs a first update of the stress, back-stress ratio, and fabric tensors. Subsequently, a more accurate estimation is computed through the second-order accurate Modified Euler procedure, and the local truncation error R_n is evaluated as the norm of the difference between the increments calculated using modified Euler and forward Euler techniques, normalised to the norm of the variable itself. The subincrement is accepted if $R_n \leq STOL$, where STOL $= 1 \times 10^{-7}$; otherwise, it is rejected. In the former case, the next pseudo-time step is calculated as $\Delta T_{n+1} = q \Delta T_n$. The variable q is calculated as $q = 0.8 \sqrt{STOL/R_n}$, and must satisfy the conditions $q \leq \sqrt{STOL/R_n}$ and $0.1 \leq q \leq 0.5$ (Sloan et al., 2001; Anandarajah, 2011). It is worth noting that a value $\Delta T_{min} = 1 \times 10^{-3}$ is assumed for robustness as the minimum allowable pseudo-time subincrement.

Using explicit schemes, it is well known that under plastic loading, the consistency condition, written as $\dot{f} = 0$ (f being the yield function), is not ensured. This is an issue known as the yield surface drift. Therefore, it is convenient to set a stress correction procedure to force the stress state lying on the yield surface: in the present study, the solution developed by Sloan et al. (2001) was implemented. It is worthwhile to mention that before applying the stress correction, the current mean effective pressure is evaluated. If the condition $p' < p_{min}$' holds, the stress tensor is forced to be hydrostatic with elements along the diagonal equal to p_{min}', whereas the back-stress ratio tensor, $\boldsymbol{\alpha}$, translates to a

quantity equal to the difference between the stress at the previous step and the hydrostatic stress tensor. The stress correction algorithm starts considering the initial values of stress $\boldsymbol{\sigma}_o$, back-stress ratio $\boldsymbol{\alpha}_o$ and fabric tensor $\mathbf{F}_o$ and a given strain increment $\Delta \varepsilon$ together with an initial pseudo-time step $\Delta T_1 = 1$. The procedure developed by Dowell and Jarratt (1972) was employed to deduce the yield surface intersection. The solution is calculated accordingly by defining $\Delta\boldsymbol{\sigma}$, $\Delta\boldsymbol{\alpha}$, and $\Delta\mathbf{F}$, and if the tolerance STOL is not exceeded, then the subincrement is accepted; otherwise, a smaller step size is considered. Once the solution is accepted, the yield surface is updated by using the committed stress and hardening variables. The end of the integration procedure for the single step is reached once $\Sigma\Delta T = 1$.

On the other hand, the 4th-order Runge-Kutta integration scheme is a four-stage method that provides 4th-order accuracy. This feature implies a computationally more demanding algorithm. It computes the stress correction for avoiding the yield surface drift, as described for the explicit schemes, with no internal substepping.

3.3. Use of NTUASand02 in finite element analysis

NTUASand02 is a multiaxial material that can be assigned to hexahedral or tetrahedral brick elements (three-dimensional conditions) or quadrilateral elements (plane-strain conditions). Using the Tcl programming language to script the finite element model in OpenSees, NTUASand02 is defined through the following command line:

```
nDMaterial NTUASand02 $matTag $nu $VoidRatio $Mc
$lambda_c $ecs_a
$P_atm $m $h0 $A0 $B $a1 $gamma1 $Me $k_bc $k_dc $H0
$zeta
$SoilDen <$kappa $integrationScheme>
```

in which the syntax *$Var* returns the value assigned to the parameter *Var*, and the correspondence between the terminology used above and the material parameters is listed in Table 1. The variable *$matTag* represents the material tag, while the parameters inside the Macauley brackets are optional: *$kappa* = 2.0 by default (Papadimitriou and Bouckovalas, 2002); *$integrationScheme* = 1 by default, corresponding to Modified Euler with substepping; otherwise, it can be set equal to 5 for Forward Euler, or to 4 for the 4th-order Runge-Kutta scheme.

Different response quantities can be monitored, such as the stress, strain, back-stress ratio, and fabric vectors in Voigt notation through the following command lines:

```
recorder Element -ele $nElem -time -file stress.out
stress
```
```
recorder Element -ele $nElem -time -file strain.out
strain
```
```
recorder Element -ele $nElem -time -file alpha.out
alpha
```
```
recorder Element -ele $nElem -time -file fabric.out
fabric
```

where *$nElem* represents the tag of the element which NTUASand02 is assigned to. The use of an elastic or elastic–plastic formulation of the material, both cases including the nonlinear Ramberg–Osgood relationship, can be considered by setting the *updateMaterialStage* command (see Section 3.1.1) equal to 0 or 1, respectively, as follows:

```
updateMaterialStage -material $matTag -stage 0/1
```

Finally, under dynamic loading, the development of the inertial effects in the finite element including NTUASand02 can be activated using the following syntax:

- ```
  updateMaterials -material $matTag Consolidation-
  Stage 1
  ```

4. Validation of the implementation

NTUASand02 was validated against the results of various laboratory investigations, comparing it with the predictions of different versions of the model available in other numerical codes (see Section 1). For the sake of conciseness, in the following the discussion is limited to some of the experimental data performed within the VELACS project (see Arulmoli et al., 1992) on Nevada sand, namely, three undrained monotonic triaxial tests, two drained monotonic triaxial tests, two cyclic triaxial tests and an undrained cyclic direct simple shear test. Notably, details of the integration strategy considered in the original implementation of the model and a full description of the initial conditions of the soil in the simulated tests are missing in Papadimitriou and Bouckovalas (2002).

The analyses on NTUASand02 were carried out, unless otherwise stated, using a Modified Euler scheme with substepping and drift correction. The calibration of the input parameters refers to the one proposed by Papadimitriou and Bouckovalas (2002) for Nevada sand (Table 1), while the state variables were initialised as described in Section 3.

4.1. Drained monotonic triaxial tests

Two drained monotonic triaxial tests were simulated to assess the implementation and demonstrate the ability of the model to reproduce the experimental response. These tests were used in Andrianopoulos et al. (2010a) to validate NTUA-SAND. Both laboratory tests were performed considering a confining pressure of 80 kPa and relative densities Dr = 40 % and 60 %, which correspond to void ratios of 0.73 and 0.66, respectively.

In OpenSees, the soil sample is modelled through a hexahedral element with a single-point stabilisation technique (*SSPbrick* elements, McGann et al., 2015), assigning boundary conditions that reproduce those in a drained triaxial test. In the consolidation stage, the confining pressure was applied as nodal loads. Then, an increasing vertical settlement was impressed to the top nodes of the element simulating the triaxial compression of the deviatoric stage. A load-control integrator with a Newton algorithm was employed. The flag *ConsolidationStage* was switched to 1 at the end of consolidation (see Section 3.1). Boundary conditions were enforced through the *Transformation* constraint handler

(McKenna et al., 2010), and a tolerance of 10^{-5} was used to control the convergence test. The latter was based on the maximum increment of the nodal displacements along two consecutive iterations.

Fig. 2 compares the response simulated with the proposed NTUA-Sand02 implementation in OpenSees in the axial strain-volumetric strain space, the simulations by Andrianopoulos et al. (2010a) in FLAC, and the experimental data from the VELACS project (Experimental Data). A fairly good agreement can be observed between NTUASand02 and the simulations provided by Andrianopoulos et al. (2010b). It is worth mentioning that no perfect match is expected between the curves obtained with NTUASand02 and NTUA-SAND, being the models similar but not identical. The final volumetric strain was the same at the end of the test, whereas a dilative response was observed in the simulations obtained using OpenSees only. Furthermore, both simulations provide a modest underestimation of the final volumetric strains compared to the experimental data for e = 0.66, while a reliable estimate is obtained when e = 0.73.

4.2. Undrained monotonic triaxial tests

The second step of the verification of NTUASand02 consists of the simulation of three undrained monotonic triaxial tests carried out in the VELACS project on Nevada sand with an initial void ratio of 0.66 and considering different effective confining pressures p' = 40, 80, and 160 kPa. The same tests were adopted by Papadimitriou et al. (2001) and Miriano (2010) to validate their implementations. These tests are simulated in OpenSees by adopting a *SSPbrickUP* element (McGann et al., 2015), which is a hexahedron with a single stabilised Gauss point in the centre and accounting for the hydro-mechanical coupling of the response. The displacement-control test is conducted using an explicit Newmark integrator with parameters γ and β equal to 0.5 and 0.25, respectively, and considering 10^4 steps (that is, an increment per step of the displacement applied to the top-nodes of the brick element of 10^{-4} m).

Fig. 3a compares the responses of the simulations in OpenSees, the analyses carried out by Miriano (2010) and those by Papadimitriou et al. (2001), in terms of the relationship between the deviatoric stress and the axial strain. The NTUASand02 undrained response is in a very good agreement with that associated with the code by Miriano (2010).

More specifically, a perfect correspondence between these two implementations is obtained for effective consolidation pressures of 40 kPa and 80 kPa, while slight differences emerge for p'=160 kPa. When
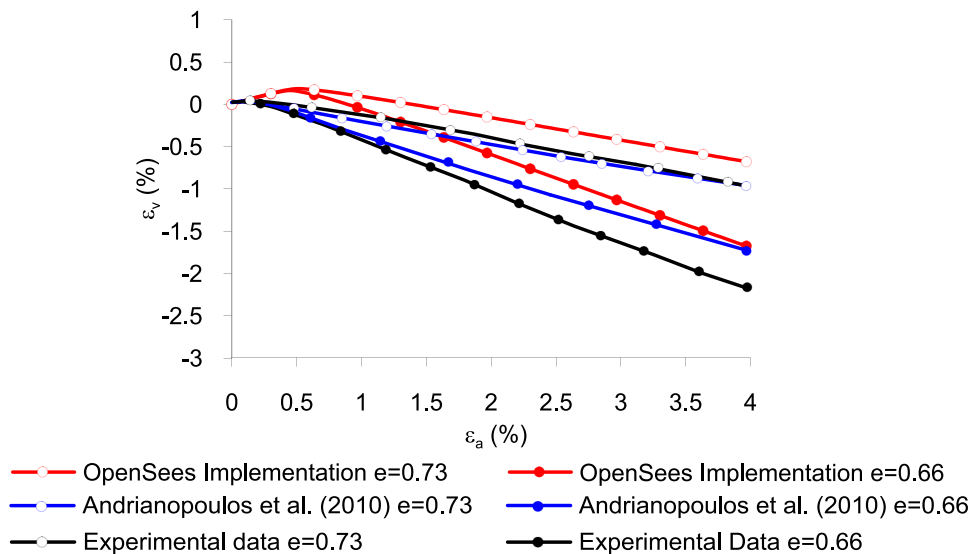
Fig. 2. Drained monotonic triaxial tests performed considering a confining pressure of 80 kPa and an initial void ratio of 0.73 and 0.66. Comparison among the experimental data, the NTUASand02 implementation in OpenSees and the simulations by Andrianopoulos et al. (2010b).
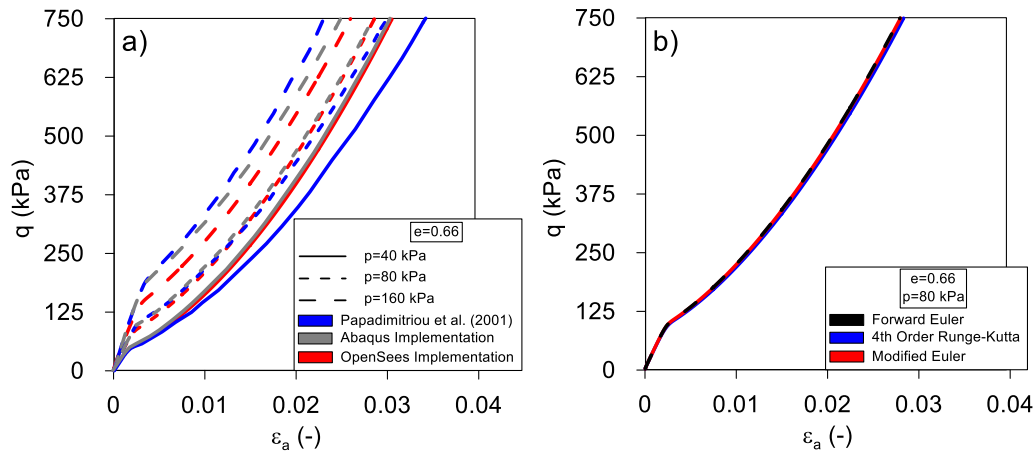
Fig. 3. (a) Comparison between the simulations of undrained monotonic triaxial tests obtained by Papadimitriou et al. (2001), in blue, Miriano (2010), in grey, and in OpenSees, in red; and (b) comparison of the use of the different integration schemes of the implemented source code. (for interpretation of the references to colour in this figure legend, the reader is referred to the web version of this article.)

comparing the NTUASand02 results with those computed through the original implementation by Papadimitriou et al. (2001), some discrepancies are more evident, although still not significant. In addition to the slightly different formulations of the two models (see Section 1), the discrepancies above are also attributed to the limited information provided in the original paper regarding the initialisation of the state variables.

Among the simulated tests, for conciseness, the one corresponding to an effective mean pressure of 80 kPa was used as a reference to validate the three implemented integration schemes: Modified Euler with stress correction and error control, Forward Euler and 4th-order Runge-Kutta. Fig. 3b demonstrates the perfect agreement between them.

4.3. Undrained cyclic direct simple shear

This section investigates the ability of NTUASand02 to simulate the behaviour of sandy soils under undrained cyclic loading. The undrained cyclic direct simple shear (DSS) test reported in Arulmoli et al. (1992) is first simulated. The load-control test is performed on a soil sample of Nevada sand with a relative density of 60 % (e = 0.66). The test considers an effective consolidation stress of 160 kPa and a shear stress in the consolidation stage of 5.9 kPa. This stress state represents the initial state for the subsequent stage, consisting of 26 cycles of harmonic shear stress with an amplitude of 13.7 kPa.

The test was simulated in OpenSees by considering a four-node

plane-strain element with hydro-mechanical coupling (*quadUP*) loaded with an appropriate combination of normal and shear forces to reproduce the experimental load pattern described above. To avoid inertial effects, an additional Rayleigh damping was introduced, which was calibrated to have a damping ratio of 10 % (Ghofrani and Arduino, 2016) in correspondence of the frequencies 0.025 and 10 Hz.

Fig. 4 shows the simulated soil response in the shear-normal stress space (τ- σ'_v) and in terms of hysteretic loops (τ- γ). The NTUASand02 response is compared with the results computed in the original work by Papadimitriou and Bouckovalas (2002) and by Miriano (2010). The latter does not start exactly from the initial conditions of the original work and the experimental test (Arulmoli et al., 1992), as the load bias was therein neglected (i.e., the shear stress at p'=160 kPa is zero instead of 5.9 kPa). The implementation in OpenSees provides a satisfactory agreement with the reference responses, particularly with the one associated with Miriano's code (2010). Both implementations exhibit a stiffer response at low strain levels compared with the original one. The response at high strain levels is well captured by NTUASand02, as well as the peculiar butterfly-shaped stress path on the occurrence of liquefaction. The moderate discrepancies are attributed to the different solution strategies adopted.

4.4. Undrained cyclic triaxial test

NTUASand02 was finally employed to simulate the undrained cyclic
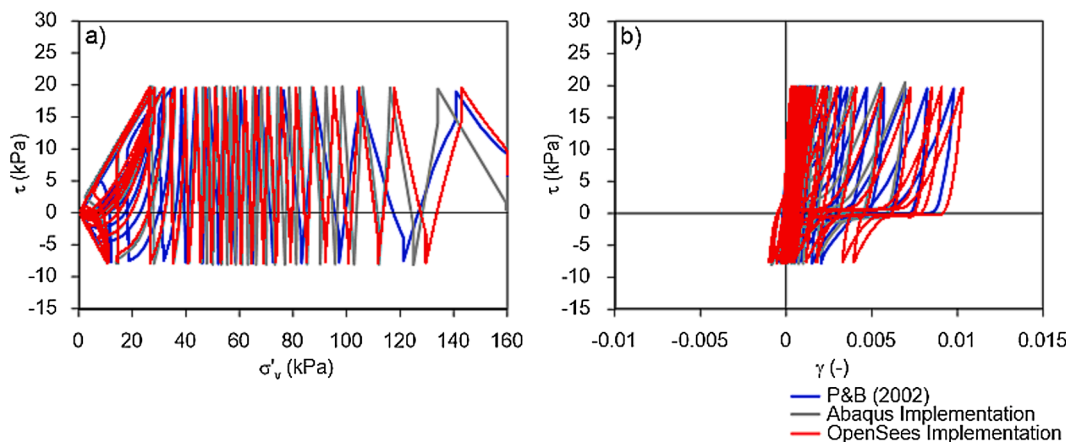
Fig. 4. (a) τ - σ'_v and (b) τ - γ relationships for the cyclic undrained DSS test carried out in Papadimitriou and Bouckovalas (2002), in blue, Miriano (2010), in grey, and in OpenSees, in red. (for interpretation of the references to colour in this figure legend, the reader is referred to the web version of this article.)

triaxial test carried out in Papadimitriou and Bouckovalas (2002). A Nevada sand sample with a void ratio of 0.66 (Dr = 60 %) was utilized in the test. In OpenSees, the material is assigned to a hexahedral finite element that has four integration points and provides a coupled hydro-mechanical response (*brickUP*-type elements). The loading process consists of an anisotropic consolidation (p'=80 kPa, q = 26 kPa), followed by the application of a cyclic deviatoric stress with amplitude q = 43.1 kPa.

The resulting stress paths and hysteresis loops obtained with NTUASand02 are compared in Fig. 5 with the simulations performed by Papadimitriou and Bouckovalas (2002), demonstrating the fairly good agreement between them. In detail, during the first cycle, NTUASand02 leads to a faster development of excess pore water pressure. Moreover, comparing the results in Figs. 4 and 5, an opposite trend can be noticed. In the former case, a slower increase in pore water pressure is provided by NTUASand02 compared to the response by Papadimitriou and Bouckovalas (2002) and vice versa for the case in Fig. 5. This lack of coherence can be ascribed to i) the different analysis approaches used, as the analysis performed in Papadimitriou and Bouckovalas (2002) considers a single-element response at constant volume while a coupled hydro-mechanical finite-element approach is employed in OpenSees, and ii) to the possible different initialisation of the earth pressure coefficient at rest (value not provided in Papadimitriou and Bouckovalas, 2002).

Fig. 6 compares the NTUASand02 response using the different integration schemes implemented. As expected, the responses overlap during the first three cycles, that is, from small- to medium-strain levels, while differences and stability issues arise on the occurrence of liquefaction (see Fig. 6c,d). However, the scatter between the results obtained using the Forward Euler and Modified Euler integration schemes can be minimized by increasing the number of steps. In terms of computational times, the Modified Euler integration scheme requires, on average, 2.89 ms per step, Forward Euler 2.64 ms per step and 4th-order Runge-Kutta runs a single step in 4.07 ms. In light of the above, the Modified Euler method with substepping appears to be the most convenient integration scheme for using NTUASand02.

In Fig. 7a,b, the stress paths and hysteretic loops of NTUASand02 are depicted together with the experimental data, while Fig. 7c,d show the time history of the excess pore water pressure ratio, r_u, and its evolution with the axial strain, respectively. Specifically, r_u is given as the ratio between the excess pore water pressure Δu and the initial vertical effective stress σ_v'. NTUASand02 can satisfactorily reproduce the experimental data, especially the evolution of r_u, except for the small-strain response for which more marked discrepancies occur. This is mainly associated with a non-optimal calibration of the input parameters of NTUASand02 (Table 1). In fact, some parameters, namely h_0 and H_0, are calibrated by means of trial-and-error. Notwithstanding, these parameters strongly affect the material response (some insights can be found in Fierro et al., 2022) and a sensitivity study on their influence, omitted for brevity, showed that the considered calibration may be significantly improved.

4.5. Shear modulus decay curve

As an essential ingredient for assessing the capability of a constitutive model to describe the dynamic response of soils from small- to large-strain levels, the shear modulus decay curve provided by the implemented NTUASand02 is now discussed. To investigate the evolution of the shear modulus, G_s, with the shear strain, γ, using the reference calibration (Table 1), cyclic tests on a volume element under drained triaxial and simple shear conditions were carried out. The analyses are named Cyclic Triax and Cyclic DSS, respectively. The finite element is described by a *SSPbrick* hexahedron and each analysis consists of a series of cyclic tests, each characterised by an increased amplitude of the input. An effective mean pressure p'=180 kPa is taken as the consolidation stress. For the Cyclic Triax analysis the secant shear modulus is determined as $\Delta q/(2(1+\nu)\Delta\varepsilon_a)$, where Δq and $\Delta\varepsilon_a$ are the amplitudes of the deviatoric stress and axial strain in each test, respectively, whereas the shear strain is calculated as $\gamma = \Delta\varepsilon_a(1+\nu)$; as per the Cyclic DSS analysis, the G_s/G_{max}- γ relationship derives directly from the response quantities.

In Fig. 8, the resulting evolutions of the secant shear modulus, G_s, normalised with respect to the relative small-strain value $G_{s,max}$, obtained with the Cyclic Triax and Cyclic DSS analyses (continuous and dashed red lines, respectively) are compared with the experimental data provided in Arulmoli et al. (1992) for Nevada sand and with the curves obtained numerically by Papadimitriou and Bouckovalas (2002), P&B. The variability of the shear modulus with the shear strain appears well simulated by the proposed implementation of NTUASand02 up to γ = 0.01 %, corresponding to G_s/G_{max} = 0.85. For larger amplitudes, the normalized shear modulus is underestimated by NTUASand02, even compared to the implementation of Papadimitriou and Bouckovalas (2002), confirming again the need for a more accurate calibration procedure of the model parameters under cyclic loading.

The analysis setting plays a role as well. Compared to triaxial conditions, the Cyclic DSS analysis leads to moderate underestimation of the normalized shear modulus for shear strains $\gamma > 0.01$ %, with maximum differences of 13 %. Overall, the cyclic triaxial test matches better the experimental data.

5. Use of the implemented NTUASand02 to determine the seismic response of a saturated soil deposit

Considering the experimental data obtained with the geotechnical
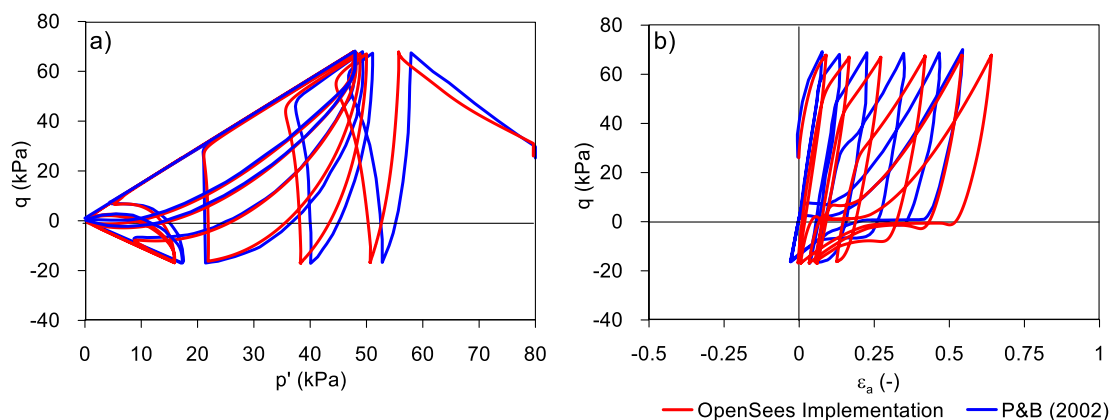
Fig. 5. (a) Stress paths in the p'-q space and (b) hysteresis loops obtained by Papadimitriou and Bouckovalas (2002), in blue, and through the OpenSees implementation, in red. (for interpretation of the references to colour in this figure legend, the reader is referred to the web version of this article.)
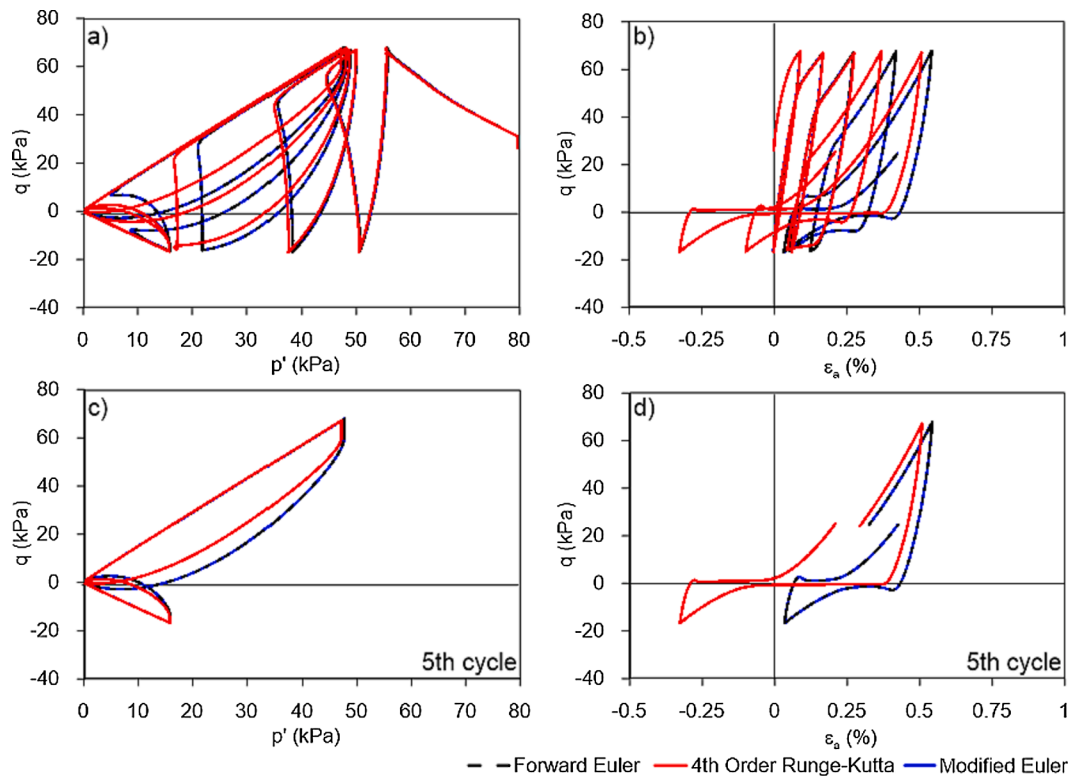
Fig. 6. Comparison between the stress paths and the hysteretic loops obtained with the proposed NTUASand02 implementation considering different integration schemes for (a,b) the entire analysis and (c,d) when liquefaction is attained.
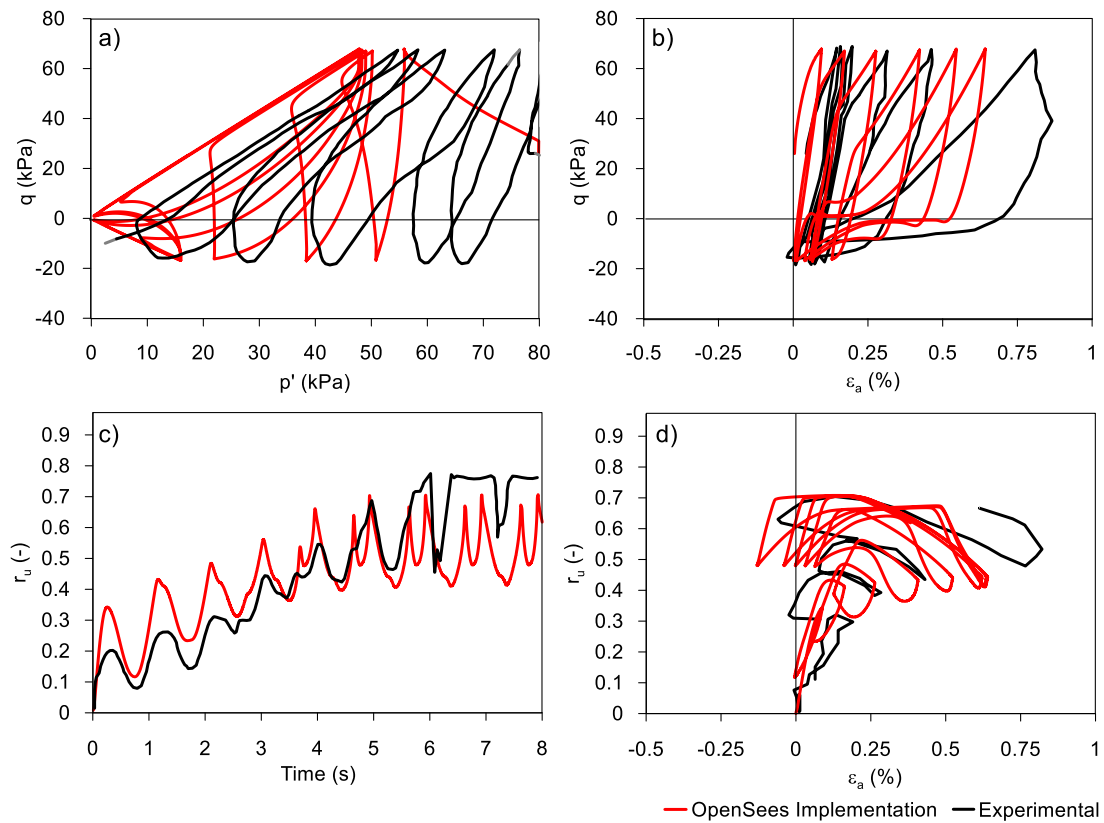
Fig. 7. (a) Stress paths in the p'-q space, (b) hysteresis loops, (c) excess pore water pressure ratio time history, and (d) its evolution with the axial strain obtained from experimental data (Arulmoli et al., 1992), in black, and using the new material in OpenSees, in red. (For interpretation of the references to colour in this figure legend, the reader is referred to the web version of this article.)
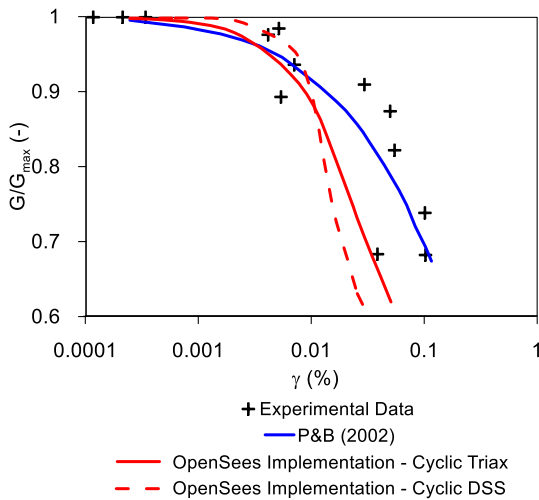
Fig. 8. Comparison among the normalised shear modulus reduction curve obtained in OpenSees, in red, using both cyclic triaxial and direct simple shear tests, the experimental data by Arulmoli et al. (1992), in black, and the data reported in Papadimitriou and Bouckovalas (2002), blue line. (for interpretation of the references to colour in this figure legend, the reader is referred to the web version of this article.)

centrifuge Model Test No.1 realised within the VELACS project, the ability of the implemented constitutive model to simulate the site effects in a liquefiable soil deposit was investigated.

In the present study, the original formulation of the fabric tensor evolution of NTUASand02 was amended with the following key aspect improving the model response and the numerical stability at liquefaction in boundary value problems. In detail, in the evolution law of the deviatoric part of the fabric tensor $\mathbf{f}$, defined as:

$$d\mathbf{f} = -H\langle -d\varepsilon_v^p \rangle [C\mathbf{n} + \mathbf{f}] \tag{7}$$

C, originally taken as a variable $C = \max\left|f_p\right|^2$, is now assumed as a parameter equal to 5 for avoiding too rapid variations of $\mathbf{f}$ when liquefaction occurs, causing in turn anomalous hardening responses and convergence issues. This feature ameliorates the cyclic response, at the cost of the additional model constant C requiring trial-and-error calibration.

Furthermore, in the modified version of NTUASand02 the Lode angle θ was implemented as $\cos(3\theta) = \sqrt{6} \cdot \mathrm{tr}\mathbf{n}^3$. This represents an equivalent expression to the one in Papadimitriou and Bouckovalas (2002), expressed explicitly in terms of the unit-norm deviatoric stress ratio $\mathbf{n}$, thus avoiding numerical instabilities under complex loading paths. The use of a constant C coefficient was previously proposed by Miriano (2010) and Miriano et al. (2016) to investigate the seismic response of a diaphragm wall; in that case it was taken equal to 130.

The modified formulation of NTUASand02 (named Modified NTUASand02 from here onwards) is employed to simulate the seismic
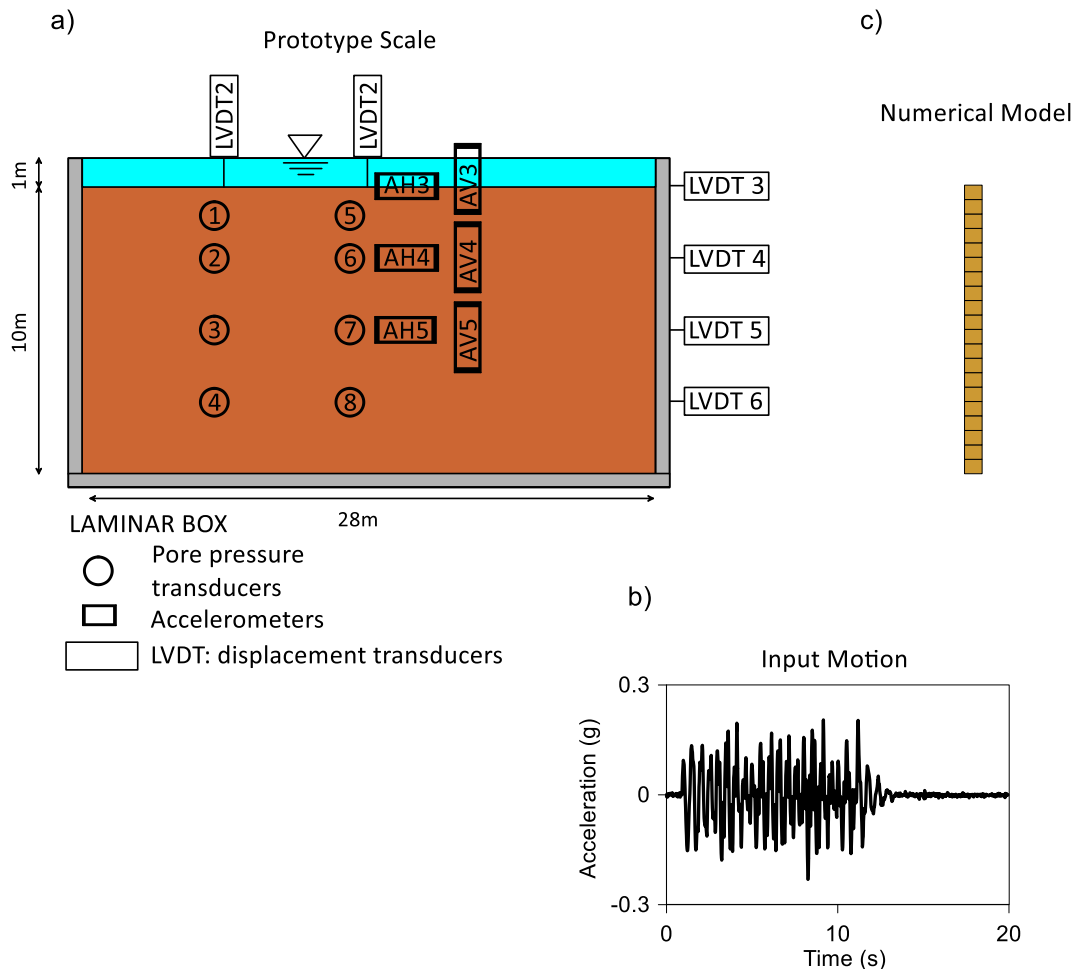
Fig. 9. (a) Schematic layout of the centrifuge model Test No.1 of the VELACS project (lengths at the prototype scale), (b) acceleration time history applied to the base of the model; (c) 1D soil column implemented in OpenSees.

response of the saturated soil deposit of Test No. 1 (Taboada and Dobry, 1994; Andrianopoulos et al., 2010b; Limnaiou and Papadimitriou, 2022). At the prototype scale, the case study is shown in Fig. 9a. It consists of a 10 m soil deposit of Nevada sand with a relative density Dr = 40 %, which corresponds to a void ratio e = 0.73. The permeability coefficient is k = 2.1 × 10^{-5} m/s, while the water table is located 1 m above the ground level. The centrifuge model was instrumented with eight pore water pressure transducers, four horizontal accelerometers, four vertical accelerometers, two vertical linear variable differential transformers (LVDT), and four horizontal LVDTs to monitor the response along the vertical axis of the model and closer to the lateral boundaries. The deposit was subjected to the acceleration time history in Fig. 9b, having a duration of 19.3 s and a PGA of 0.235 g. The seismic input is approximately sinusoidal with a predominant frequency of about 2 Hz.

The free-field site response of the case study was reproduced in OpenSees at the prototype scale by implementing the one-dimensional soil column in Fig. 9c. It is composed of twenty 0.5 m × 0.5 m quadrilateral elements providing a coupled hydro-mechanical response, named *SSPquadUP* in the OpenSees framework (McGann et al., 2012), including the Modified NTUASand02.

Impervious boundaries were assigned at the bottom and laterally (the water flow points to the ground level). The base nodes are fixed in the vertical direction and are subjected to the considered seismic input in the horizontal one. The nodes along the column can displace horizontally and vertically, and those at the same elevation are constrained to undergo the same displacement. A pore water pressure of 9.81 kPa and an equal, compensating vertical pressure were applied to simulate the position of the ground water table at an elevation of 1 m.

To compare the performance of the Modified NTUASand02 with models available in the literature, an additional dynamic analysis was carried out by considering the widely used SANISAND model (Dafalias and Manzari, 2004), implemented in OpenSees by Ghofrani and Arduino (2016). The material parameters selected for the Modified NTUASand02 are reported in Table 1, with parameter B = 520 as in Papadimitriou and Bouckovalas (2002). On the other hand, the calibration carried out by Taiebat et al. (2010) for Nevada sand was adopted for SANISAND, corresponding however to a lower small-strain stiffness exhibited by SANISAND compared to the considered one in the test. The relative list of parameters is reported in Table 2. The initial void ratio was set equal to 0.724, corresponding to Dr = 45 % (Andrianopoulos et al., 2010b).

The permeability at the model scale corresponds to 2.1 × 10^{-5} m/s, whereas the permeability at the prototype scale was taken as *N* times the former one, where *N* is the multiplier of the gravity acceleration used in the centrifuge test. As a result, k was set equal to 1.05 × 10^{-3} m/s (Andrianopoulos et al., 2010b). A small Rayleigh damping was introduced in the numerical analyses to attenuate spurious effects at high frequencies. The Rayleigh damping formulation was calibrated to have a damping ratio of 3 % in correspondence of the frequencies 2 Hz and 20

Hz, corresponding approximately to the significant first and third natural frequencies of the soil column.

The responses of the Modified NTUASand02 and SANISAND are compared with the experimental data in Figs. 10 and 11 in terms of acceleration time histories and excess pore water pressure ratio $r_u = \Delta u/\sigma'_{vo}$, respectively. The proposed implementation reproduces satisfactorily the highly nonlinear response observed experimentally. In terms of acceleration time histories at the two considered depths z = 2.5 and 5 m, the proposed code and SANISAND provide very similar results. At z = 2.5 m, the analysis with the former shows some unrealistic peaks in a very narrow time interval. Nonetheless, this inaccuracy occurs when the soil exhibits pronounced liquefaction and localises near the ground level only.

As per the excess pore water pressure, the proposed code is able to simulate realistically the time evolution of r_u in close proximity to the ground level, while some major discrepancies occur at z = 5 m. The Modified NTUASand02 captures well the progressive increase of the pore water pressure up to 6.5 s but underestimates the residual value of about 60 %. By contrast, the SANISAND response is affected by significant oscillations of r_u in the entire soil volume interested by liquefaction, and a slightly faster development of excess pore water pressure, indicating the promising response of the Modified NTUASand02. The discrepancies between numerical simulations and experimental data magnify after *5 s*, that is about when the superficial soil starts experiencing liquefaction. This is an expected result as the considered constitutive models are not particularly prone to capture the postliquefaction behaviour.

6. Concluding remarks

The paper described the workflow related to the implementation of the advanced, bounding surface constitutive model NTUASand02 (Papadimitriou and Bouckovalas, 2002) in the open-source, finite element analysis framework OpenSees, including an essential validation of the model against available experimental data and previous implementations. Compared to the latter ones, mainly developed in independent constitutive drivers or introducing simplifying assumptions in the constitutive response for implementation purposes, this paper contributes to make widely available an efficient model for describing the meso-scale behaviour of coarse-grained soils in a variety of earthquake engineering problems, such as liquefaction triggering, ground response and soil-structure interaction analysis under complex conditions, seismic assessment of slopes. NTUASand02 can work under plane-strain and three-dimensional conditions. Several integration schemes were implemented to address with flexibility the incremental response of the model according to the specific boundary value problem under examination. NTUASand02 was tested in a number of laboratory tests under monotonic and cyclic loading to evaluate the effectiveness of the implementation in OpenSees and also the ability of the model to simulate the soil response under a wide range of loading conditions at the finite element level.

It was demonstrated that NTUASand02 can realistically simulate the evolution of the pore water pressure under undrained conditions from small-strain levels up to the attainment of the soil strength. In particular, the simulations in the case of monotonic and cyclic triaxial tests showed excellent results, with some slight differences compared with the benchmark case studies mainly attributed to the different numerical environments used. More evident discrepancies with available codes occur in a direct simple shear mode, although the identification of the relative causes cannot be objectively assessed because of the lack of complete information about initial conditions and the problem settings of the simulated tests. Finally, it was shown that the implemented constitutive model is able to simulate efficiently site effects and the occurrence of liquefaction in boundary value problems. The dynamic analyses highlighted a good agreement with available experimental data in a broad range of strains.

Table 2
Assumed set of parameters of the SANISAND model (Taiebat et al., 2010).

Parameter	Meaning	Value
G_0	Elastic material constant	150
ν	Poisson's ratio	0.05
M^c	Critical-state stress ratio	1.14
c	Ratio of critical-state stress ratio in extension and compression	0.78
λ_c	State line constant	0.027
e_0	Void ratio at p' = 0	0.83
ξ	State line constant	0.45
h_0	Plastic modulus constant	9.7
c_h	Plastic modulus constant	1.02
n^b	Plastic modulus constant	2.56
A_0	Dilatancy constant	0.81
n^d	Dilatancy constant	1.05
z_{max}	Fabric-dilatancy tensor parameter	5.0
c_z	Fabric-dilatancy tensor parameter	800
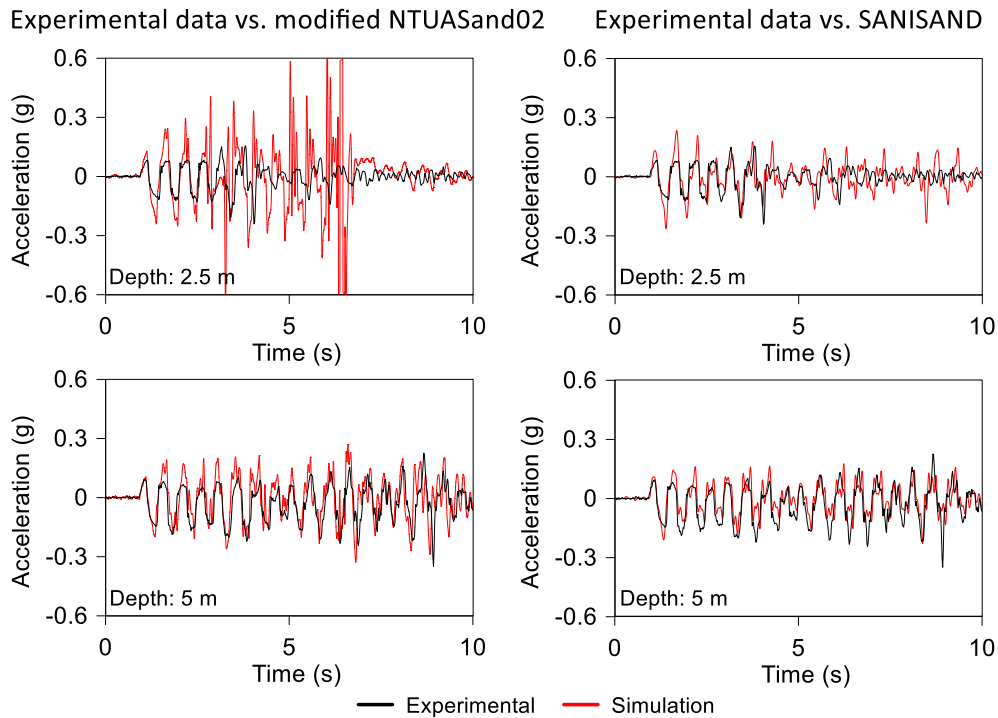
Fig. 10. Experimental vs. simulated acceleration time-series at 2.5 m and 5 m below the ground level considering Modified NTUASand02 and SANISAND.
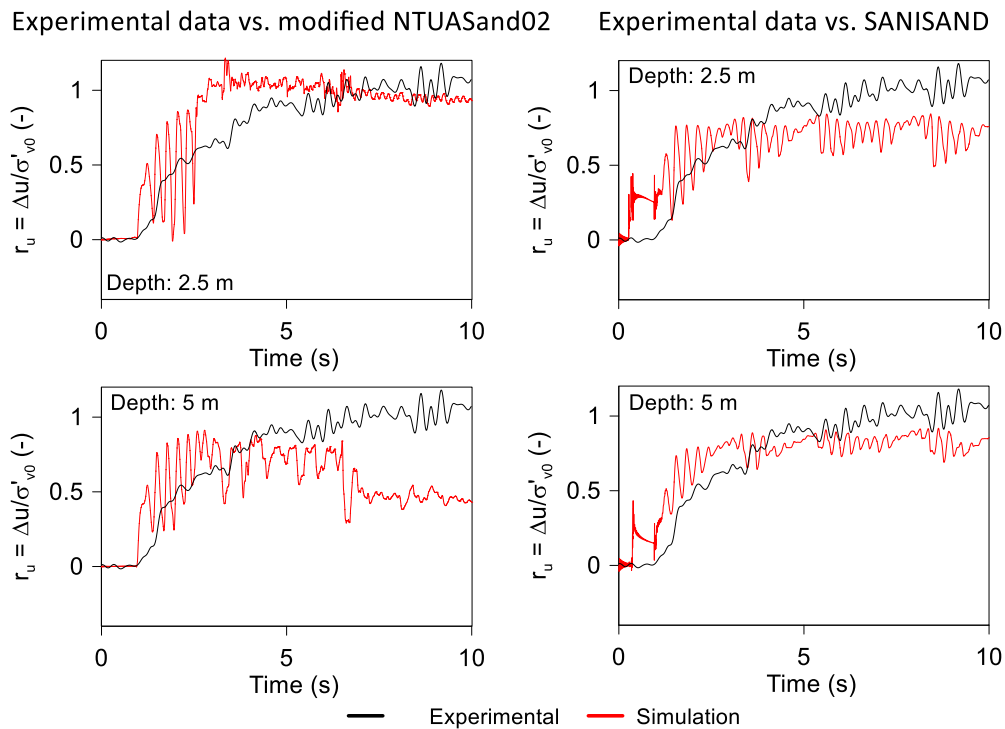
Fig. 11. Experimental vs. simulated excess pore water pressure ratio time-series at 2.5 m and 5 m below the ground level considering NTUASand02 and SANISAND.

The necessary ingredients for the utilization of NTUASand02 in finite element analyses using OpenSees were provided. The description of the implementation workflow of the new source code allows users to readily extend it with the latest developments in the field, promoting an open-source use of advanced geomechanics in large-scale finite element applications.

CRediT authorship contribution statement

Tony Fierro: Conceptualization, Methodology, Software, Valida-tion, Formal analysis, Investigation, Data curation, Writing – original draft. **Stefano Ercolessi:** Software, Validation, Formal analysis, Writing – review & editing. **Davide Noè Gorini:** Conceptualization, Methodol-ogy, Software, Validation, Formal analysis, Writing – review & editing, Supervision. **Giovanni Fabbrocino:** Conceptualization, Supervision,

Resources, Writing – review & editing. **Filippo Santucci de Magistris:** Conceptualization, Methodology, Resources, Writing – review & editing, Supervision.

Declaration of competing interest

The authors declare that they have no known competing financial interests or personal relationships that could have appeared to influence the work reported in this paper.

Data availability

Data will be made available on request.

Acknowledgements

This study was partly developed as a contribution of the University of

Appendix A. Functions composing the new source code in OpenSees

The main file of the NTUASand02 source code contains methods (i.e., C++ functions or subroutines belonging to the same class that execute a prescribed instruction) that are useful for defining the elastic–plastic response. The latter can be grouped as follows:

- Full constructor: it assigns the initial values to the material constants. In addition to the input parameters, those defining the type of integration scheme adopted in the finite element analysis are provided.
- Methods called when convergence is achieved at the generic analysis step, i.e., *commitState*, *revertToLastCommit* and *revertToStart*. The former defines the committed state variables during plastic loading (such as void ratio and/or stress, back-stress ratio, fabric tensors); *revertToLastCommit* is used to keep the internal variables unchanged during neutral loading or unloading; and *revertToStart* allows the user to set the internal variables to the initial values during the analysis (particularly useful in staged analyses).
- Methods handling the material response, such as *getType*, *getOrder*, *getCopy*, and *getStressToRecord*. The former ones are related to the problem type (i.e., plane-strain or three-dimensional); *getCopy* creates a new instance by cloning an object (e.g., a material object to be assigned to an element provides a clone of itself to the calling element), while *getStressToRecord* sends committed values to the finite element.
- Method *initialize:* the method initialises the member variables, consisting of the material constants, the tensors describing the state of the material and the variables related to the integration schemes.
- Methods *setResponse* and *getResponse* handle the output quantities recorded in the analysis, that is, the stresses, total and elastic strains, back-stress ratio and fabric tensors, while method *Print* sends back the material tag, material name, and material parameters to the output stream.
- Methods *sendSelf* and *recvSelf* are essential for using the material with parallel computing because they allow parallel processes communicating during the analysis. In *sendSelf*, all variables of the materials are defined, and during the analysis, they are sent to the other processes running in parallel, and then *recvSelf* returns the committed information.
- Methods *setParameter* and *updateParameter* allow for the reassignment of a parameter in different stages of the analysis.
- Virtual methods that aim at sending back elastic and plastic strain tensors (*getEStrain* and *getPStrain*), stress tensor (*getStress*), tangent stiffness tensor (*getTangent*), current material state (*getState*), back-stress ratio tensor (*getAlpha*) and fabric tensor (*getFabric*).

Additional functions were implemented for computing the updated material state within the iterative procedure at each analysis step. In particular, the function *g* calculates the interpolation function that accounts for the effect of the Lode angle in the definition of the wedge-shaped surface, while the yield surface is defined using the function *GetF*. The state parameter is calculated using the method *GetPsi*, while the normal to the yield surface is determined using *GetNormalToYield*. The elastic moduli are calculated through *GetElasticModuli*. This method evaluates whether the first shearing occurs or if the material has just experienced a shear reversal, to compute the value of *T* accordingly (see Section 2). To this end, an additional variable called *mConsolidationStage* was implemented in the code. When it is set to 0, a gravity analysis is performed, whereas the system is subjected to dynamic loading when *mConsolidationStage* = 1. Through parsing from the script including the OpenSees finite element model, the latter variable can be updated at the end of the gravity analysis. In this manner, the eventual early identification of shear reversals is avoided, and no further tolerances to detect this phenomenon under cyclic loading are needed. Then, the *GetLodeAngle* method determines the current Lode Angle in terms of invariants.

The calculation of the incremental response requires another fundamental method, named *GetStateDependent*. It applies the mapping rule to find the distance of the current back-stress ratio from the wedge-shaped surfaces controlling the hardening response (see Section 2) and evaluates the plastic flow. To this end, the stress ratios $M_{c,e}^{(b,c,d)}$ and the interpolation functions α_θ^i (Eq. (3)) are computed to obtain the image back-stress ratios (Eq. (2)). Finally, the scalar variable h_f (Eq. (4)) accounting for the fabric evolution and the magnitude of plastic volumetric strains is determined.

References

Anandarajah, A., 2011. Computational methods in elasticity and plasticity: solids and porous media. Springer-Verlag, New York, New York.

Andrianopoulos, K.I., Papadimitriou, A.G., Bouckovalas, G.D., 2010a. Explicit integration of bounding surface model for the analysis of earthquake soil liquefaction. Int. J. Numer. Anal. Meth. Geomech. 34 (15), 1586–1614.

Andrianopoulos, K.I., Papadimitriou, A.G., Bouckovalas, G.D., 2010b. Bounding surface plasticity model for the seismic liquefaction analysis of geostructures. Soil Dyn. Earthq. Eng. 30 (10), 895–911.

Arulmoli, K., Muraleetharan, K.K., Hossain, M.M., Fruth, L.S., 1992. VELACS verification of liquefaction analyses by centrifuge studies -Laboratory Testing Program – Soil Data Report, Research Report, The Earth. Technology Corporation.

Been, K., Jeffries, M.G., 1985. A state parameter for sands. Geotechnique 41, 365–381.

Boulanger, R.W., Ziotopoulou, K., 2019. A constitutive model for clays and plastic silts in plane-strain earthquake engineering applications. Soil Dyn. Earthq. Eng. 2019 (127), 105832 https://doi.org/10.1016/j.soildyn.2019.105832.

Boulanger, R.W., Ziotopoulou, K., 2017. PM4Sand (version 3.1): A sand plasticity model for earthquake engineering applications. Report No. UCD/CGM17/01, Center for Geotechnical Modeling, Department of Civil and Environmental Engineering, University of California, Davis, CA, March, 112 pp.

Brinkgreve, R.B.J., Engin, E., Swolfs, W.M., 2021. Plaxis V21.01 2021. Delft, Plaxis bv.

Chaloulos, Y.K., Bouckovalas, G.D., Karamitros, D.K., 2013. Pile response in submerged lateral spreads: Common pitfalls of numerical and physical modeling techniques. Soil Dyn. Earthq. Eng. 55, 275–287.

Chaloulos, Y.K., Bouckovalas, G.D., Karamitros, D.K., 2014. Analysis of liquefaction effects on ultimate pile reaction to lateral spreading. J. Geotech. Geoenviron. Eng. 140 (3), 04013035.

Chen, L., Arduino, P., 2021. Implementation, verification and validation of the PM4Sand model in OpenSees. PEER Report No. 2021/02. Pacific Earthquake Engineering Research Center Headquarters, University of California, Berkeley, March 2021.

Dafalias, Y.F., 1986. Bounding surface plasticity. I: mathematical foundation and hypoplasticity. J. Eng. Mech. 112, 966–987. https://doi.org/10.1061/(ASCE)0733-9399(1986)112:9(966).

Dafalias, Y.F., Manzari, M.T., 2004. Simple plasticity sand model accounting for fabric change effects. J. Eng. Mech. 130, 622–634. https://doi.org/10.1061/(ASCE) 0733-9399 130:6(622).

Dafalias, Y.F., Popov, E.P., 1975. A model of nonlinearly hardening materials for complex loadings. Acta Mech. 21, 173–192.

Dimitriadi, V.E., Bouckovalas, G.D., Papadimitriou, A.G., 2017. Seismic performance of strip foundations on liquefiable soils with a permeable crust. Soil Dyn. Earthq. Eng. 100, 396–409.

Dimitriadi, V.E., Bouckovalas, G.D., Chaloulos, Y.K., Aggelis, A.S., 2018. Seismic liquefaction performance of strip foundations: effect of ground improvement dimensions. Soil Dyn. Earthq. Eng. 106, 298–307.

Dowell, M., Jarratt, P., 1972. The Pegasus method for computing the root of an equation. BIT 12, 503–508.

Fierro, T., 2022. Implementation and use of advanced constitutive models in numerical codes for the evaluation of the soil response under seismic loadings. University of Molise (Ph.D. Thesis).

Fierro, T., Gorini, D.N., Castiglia, M., Santucci de Magistris, F., 2022. Implementation and Use of the Bounding Surface Plasticity Geomaterial NTUASand 02. In: Eurasian Conference on OpenSees 2022 Jul 7, pp. 334–343. Cham: Springer Nature Switzerland.

Ghofrani, A., 2018. Development of Numerical Tools For the Evaluation of Pile Response to Laterally Spreading Soil. The University of Washington, Seattle (Ph.D. Thesis).

Ghofrani, A., Arduino, P., 2016. Prediction of LEAP centrifuge test results using a pressure-dependent bounding surface constitutive model. Soil Dyn. Earthq. Eng. https://doi.org/10.1016/j.soildyn.2016.12.001.

Ishihara, K., Tatsuoka, F., Yasuda, S., 1975. Undrained deformation and liquefaction of sand under cyclic stresses. Soils Found. 15 (1), 29–44.

Itasca Consulting Group, Inc., 2019. FLAC — Fast Lagrangian Analysis of Continua, Ver. 8.1. Minneapolis: Itasca.

Karamitros, D.K., Bouckovalas, G.D., Chaloulos, Y.K., Andrianopoulos, K.I., 2013a. Numerical analysis of liquefaction-induced bearing capacity degradation of shallow foundations on a two-layered soil profile. Soil Dyn. Earthq. 44, 90–101.

Karamitros, D.K., Bouckovalas, G.D., Chaloulos, Y.K., 2013b. Insight into the seismic liquefaction performance of shallow foundations. J. Geotech. Geoenviron. Eng. 139 (4), 599–607.

Limnaiou, T.G., Papadimitriou, A.G., 2022. Verification of bounding surface plasticity model with reversal surfaces for the analysis of liquefaction problems. Soil Dyn. Earthq. Eng. https://doi.org/10.1016/j.soildyn.2022.107394.

Ling, H.I., Liu, H., 2003. Pressure-level dependency and densification behavior of sand through generalized plasticity model. J. Eng. Mech., ASCE 129 (8), 851–860.

Manzari, M.T., Dafalias, Y.F., 1997. A critical state two-surface plasticity model for sands. Geotechnique 47 (2), 255–272.

Marinatou, S.M., Zontanou, V.A., Chaloulos, Y.K., Bouckovalas, G.D., 2017. Liquefaction induced uplift of pipelines: numerical modeling and parametric analyses. In: Taiebat, M., Wijewickreme, D., Athanasopoulos-Zekkos, A., Boulanger, R.W. (Eds.) Proceedings of the 3rd International Conference of Performance-Based Design in Earthquake Geotechnical Engineering, Vancouver, BC, USA, July 2017.

Martinelli, M., Miriano, C., Tamagnini, C., Masin, D., 2015. Implementation of SANISAND model as ABAQUS umat and PLAXIS user defined subroutines.

Mašín, D., 2014. Clay hypoplasticity model including stiffness anisotropy. Géotechnique 64 (3), 232–238.

McGann, C.R., Arduino, P., Mackenzie-Helnwein, P., 2012. Stabilized single-point 4-node quadrilateral element for dynamic analysis of fluid saturated porous media. Acta Geotech. 7 (4), 297–311.

McGann, C.R., Arduino, P., Mackenzie-Helnwein, P., 2015. A stabilized single-point finite element formulation for three-dimensional dynamic analysis of saturated soils. Comput. Geotech. 66, 126–141.

McKenna, F., Scott, M.H., Fenves, G.L., 2010. OpenSees, Nonlinear finite-element analysis software architecture using object composition. J. Comput. Civil Eng. 24 (1), 95–107.

Miriano, C., 2010. Numerical Modelling of the Seismic response of Flexible Retaining Structures. Sapienza University of Rome (in Italian, Ph.D. Thesis).

Miriano, C., Cattoni, E., Tamagnini, C., 2016. Advanced numerical modeling of seismic response of a propped r.c. diaphragm wall. Acta Geotech. 11, 161–175. https://doi.org/10.1007/s11440-015-0378-8.

Niemunis, A., Herle, I., 1997. Hypoplastic model for cohesionless soils with elastic strain range. Mech. Cohesive-Frictional Mater. 2, 279–299.

Papadimitriou, A.G., Bouckovalas, G.D., Dafalias, Y.F., 2001. Plasticity model for sand under small and large cyclic strains. J. Geotech. Geoenviron. Eng. ASCE 127 (11), 973–983.

Papadimitriou, A.G., Bouckovalas, G.D., 2002. Plasticity model for sand under small and large cyclic strains: a multiaxial formulation. Soil Dyn. Earthq. Eng. 22, 191–204.

Papadimitriou, A.G., Chaloulos, Y.K., Dafalias, Y.F., 2019. A fabric-based sand plasticity model with reversal surfaces within Anisotropic Critical State Theory. Acta Geotech. 14 (2), 253–277.

Papadimitriou, A., Tsepelidou, N., Sideris, A., Pavlopoulou, A., Katsoularis, V., 2021. Seismic soil liquefaction under shallow founded structures and its mitigation in urban environments. In: EGU General Assembly Conference Abstracts, pp. EGU21-4620.

Papadimitriou, A.G., Valsamis, A.I., Limnaiou, T.G., 2022. Liquefaction mitigation methods for existing shallow-founded elongated structures on horizontal or mildly-inclined ground. Soil Dyn. Earthq. Eng. 162, 107453.

Pastor, M., Zienkiewicz, O.C., Chan, A.H.C., 1990. Generalized plasticity and the modeling of soil behaviour. Int. J. Numer. Anal. Meth. Geomech. 14 (3), 151–190.

Prevost, J.H., 1978. Plasticity theory for soil stress-strain behaviour. J. Eng. Mech. Div. 104 (5), 1177–1194.

Schofield, A., Wroth, P., 1968. Critical State Soil Mechanics. McGraw-Hill, USA.

Sloan, S.W., Abbo, A.J., Sheng, D., 2001. Refined explicit integration of elastoplastic models with automatic error control. Eng. Comput. 18 (1/2), 121–194.

Taboada, V., Dobry, R., 1994. Experimental results of model No. 1 at RPI. In: Proc. Int. Conf. Verif. Numer. Proced. Anal. Soil liq. Probl., davis, CA, 17-10, October, vol. 1, p. 3–17.

Taborda, D.M.G., Zdravković, L., Kontoe, S., Potts, D.M., 2014. Computational study on the modification of a bounding surface plasticity model for sand. Comput. Geotech. 94, 22–30.

Taiebat, M., Jeremic, B., Dafalias, Y.F., Kaynia, A.M., Cheng, Z., 2010. Propagation of seismic waves through liquefied soils. Soil Dyn. Earthq. Eng. 30, 236–257.

Yang, Z., Elgamal, A., Parra, E., 2003. Computational model for cyclic mobility and associated shear deformation. J. Geotech. Geoenviron. Eng. ASCE 129 (12), 1119–1127.

Yang, Z., Elgamal, A., 2008. Multi-surface cyclic plasticity sand model with Lode angle effect. Geotech. Geol. Eng. 26, 335–348.